

Direct Observation of Zhang-Li Torque Expansion of Magnetic Droplet Solitons

Sunjae Chung,^{1,2,3} Q. Tuan Le,^{1,2} Martina Ahlberg,^{1,4} Ahmad A. Awad,^{1,4} Markus Weigand,⁵ Iuliia Bykova,⁵ Roman Khymyn,¹ Mykola Dvornik,¹ Hamid Mazraati,^{2,4} Afshin Houshang,^{1,4} Sheng Jiang,² T. N. Anh Nguyen,^{1,2,6} Eberhard Goering,⁵ Gisela Schütz,⁵ Joachim Gräfe,⁵ and Johan Åkerman^{1,2,4,*}

¹Department of Physics, University of Gothenburg, 412 96 Gothenburg, Sweden

²Department of Applied Physics, School of Engineering Sciences, KTH Royal Institute of Technology, 164 40 Kista, Sweden

³Department of Physics and Astronomy, Uppsala University, 751 20 Uppsala, Sweden

⁴NanOsc AB, 164 40 Kista, Sweden

⁵Max Planck Institute for Intelligent Systems, 70569 Stuttgart, Germany

⁶Laboratory of Magnetism and Superconductivity, Institute of Materials Science, Vietnam Academy of Science and Technology, 18 Hoang Quoc Viet, 122300 Hanoi, Vietnam



(Received 8 February 2018; published 23 May 2018)

Magnetic droplets are nontopological dynamical solitons that can be nucleated in nanocontact based spin torque nano-oscillators (STNOs) with perpendicular magnetic anisotropy free layers. While theory predicts that the droplet should be of the same size as the nanocontact, its inherent drift instability has thwarted attempts at observing it directly using microscopy techniques. Here, we demonstrate highly stable magnetic droplets in all-perpendicular STNOs and present the first detailed droplet images using scanning transmission X-ray microscopy. In contrast to theoretical predictions, we find that the droplet diameter is about twice as large as the nanocontact. By extending the original droplet theory to properly account for the lateral current spread underneath the nanocontact, we show that the large discrepancy primarily arises from current-in-plane Zhang-Li torque adding an outward pressure on the droplet perimeter. Electrical measurements on droplets nucleated using a reversed current in the antiparallel state corroborate this picture.

DOI: [10.1103/PhysRevLett.120.217204](https://doi.org/10.1103/PhysRevLett.120.217204)

Magnetodynamical solitons [1], such as droplets [2–13] and spin wave (SW) bullets [14–19], are condensed states of SWs deriving their stability from spin precession. Their nucleation requires a high local SW density, which can be achieved in spin torque nano-oscillators (STNOs) where a current is injected into an extended giant magnetoresistance (GMR) trilayer through a nanocontact (NC) [20,21]. STNOs based on easy-plane GMR stacks [22–24] favor propagating SWs [15,17,19,25–28] when the free layer is saturated towards the film normal (the magnetodynamic nonlinearity $N > 0$) and SW bullets [14,15,17] when it is saturated towards the plane ($N < 0$). In STNOs with free layers having a large perpendicular magnetic anisotropy (PMA), $N < 0$ at all perpendicular fields and any auto-oscillation is inherently self-localized, which promotes a high local SW density [29,30]. The magnetodynamics can then condense into a magnetic droplet soliton, characterized by a reversed core and a perimeter where all spins precess with the same frequency and, in ideal conditions, with the same phase [2,3].

As all experimental realizations of droplets have so far relied on orthogonal spin valves, where the fixed layer magnetization M_p has an easy-plane anisotropy (e.g., Co or NiFe) [5,6,8–11,13], a perpendicular field had to be applied, which tilts or saturates M_p out-of-plane. The combination of a tilted M_p and a large Oersted field

subjects the droplet to a drift instability [3,9]; i.e., it leaves the NC and dissipates out after which a new droplet can form. The drift instability complicates the experimental characterization of the intrinsic droplet properties, and recent attempts at determining the droplet size, shape, and degree of reversal using scanning transmission X-ray microscopy (STXM) resulted in much smaller estimates of the reversal ($\approx 25^\circ$) than theoretically predicted ($\approx 180^\circ$), and an apparent noncircular droplet shape [31].

Here, we realize stable magnetic droplets in STNOs based on all-perpendicular spin valves and use electrical and STXM measurements to study their properties. Using both the Ni and Co edges, our STXM results show that the droplet core is essentially completely reversed ($\approx 180^\circ$) and that the droplet has a highly circular shape. The droplet is, however, almost twice as large as the NC. We show that the original droplet theory must be extended to include a fully three-dimensional current distribution exerting a spin transfer torque that not only nucleates the droplet but then pushes the droplet boundary radially away from the NC, effectively doubling its diameter.

Stacks composed of a Ta(4)/Cu(14)/Ta(4)/Pd(2) seed layer (numbers in nm), a [Co(0.35)/Pd(0.7)] \times 5/Co(0.35)/Cu(5)/[Co(0.22)/Ni(0.68)] \times 4/Co(0.22) spin valve, and a Cu(2)/Pd(2) capping layer were magnetron sputtered onto thermally oxidized Si [Fig. 1(a)]. Using

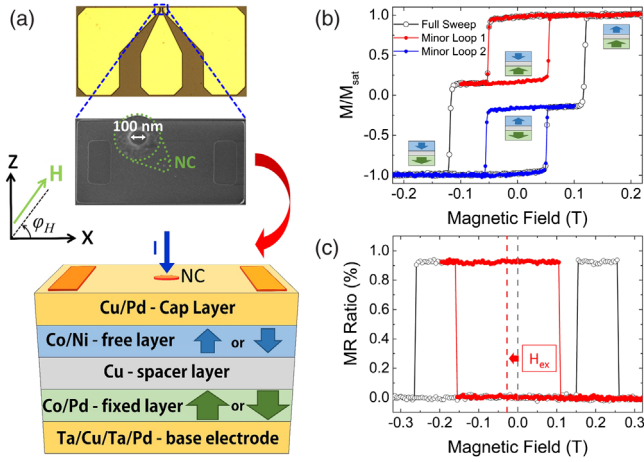


FIG. 1. (a) Schematic of an all-perpendicular STNO. The current (I_{dc}) flows through the NC fabricated on top of the stack. The magnetic field H is applied at an angle φ_H from the plane. (b) Full (black circles) and minor (red and blue dots) out-of-plane hysteresis loops of the unpatterned material stack showing decoupled free and fixed layers. (c) Full (black circles) and minor loop (red dots) low-current (-0.6 mA) magnetoresistance (MR) measurements of the STNO showing MR $\sim 1\%$ and some process induced interlayer coupling of about -0.03 T.

optical lithography, $8 \mu\text{m} \times 16 \mu\text{m}$ mesas were fabricated and insulated by a 30-nm-thick SiO_2 film using chemical vapor deposition. Electron beam lithography was used to pattern circular NCs with diameters $d_{NC} = 50\text{--}150$ nm. The SiO_2 was etched through using reactive ion etching (RIE). The STNO fabrication was completed by deposition of $\text{Cu}(500)/\text{Au}(100)$ top electrodes and lift off. For STXM compatible STNOs, a similar process was employed on 300-nm-thick LPCVD silicon nitride Si wafers, after which highly selective deep RIE removed the Si from the wafer backside to leave nitride membranes [Fig. 3(a)].

Figure 1(a) shows a schematic of the all-perpendicular STNO having a Co/Pd multilayer fixed layer and a Co/Ni multilayer free layer, both with sufficient PMA to have their remanent states along the film normal. Figure 1(b) shows major and minor out-of-plane magnetization hysteresis loops of the full unpatterned material stack, measured using alternating gradient magnetometry, with two distinct switching fields corresponding to the fixed and free layer, respectively. The symmetry of the minor loops indicate negligible coupling between the fixed and the free layers before patterning. Figure 1(c) shows a magnetoresistance (MR) hysteresis loop of a fully processed STNO having about 1% MR and 0.03 T interlayer coupling after patterning.

Figure 2(a) shows the resistance variation of a 100 nm nanocontact STNO as the drive current is swept back and forth at three different perpendicular field strengths. At a negative current of about -12 mA and in a field of 0.25 T, there is a sharp resistance step indicating the nucleation or collapse of a droplet depending on the current sweep

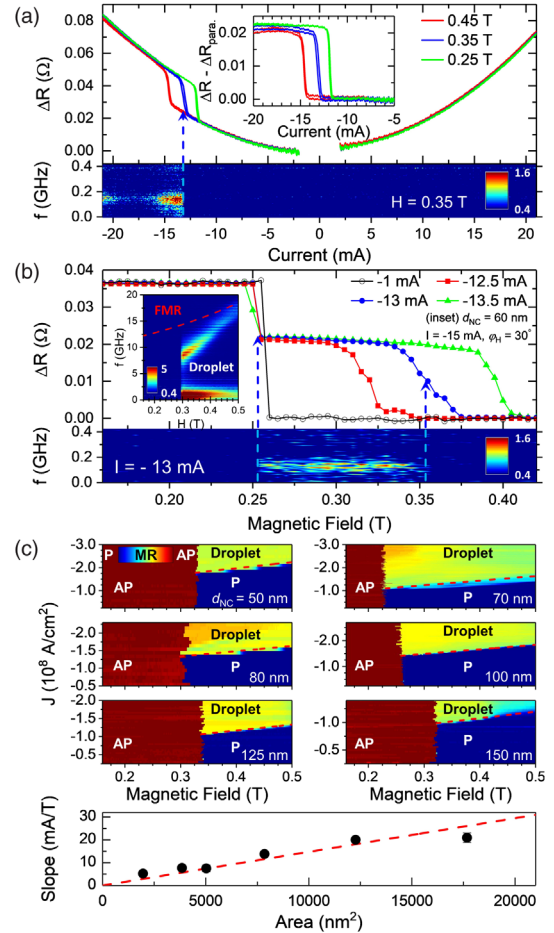


FIG. 2. (a) Change in resistance (ΔR) of a 100 nm NC vs I_{dc} showing droplet nucleation at a field-dependent negative current on a parabolic Joule heating background. Inset: same data after background subtraction. The color plot is the power spectral density (PSD) up to 0.4 GHz in a field of 0.35 T, showing how the step in ΔR is accompanied by the onset of low-frequency microwave noise. (b) ΔR vs field at different negative currents for the same NC as in (a). At a small negative I_{dc} (-1 mA), the state switches directly from AP to P at about 0.25 T. For larger negative I_{dc} , the AP state first switches to an intermediate resistance consistent with a droplet before gradually switching to the P state. The droplet is again accompanied by microwave noise. Inset: PSD in a field tilted 30° from the plane showing both the precession frequency and much broader and stronger microwave noise. (c) Field-swept ΔR measurements at different negative I_{dc} for NC diameters ranging from 50 to 150 nm, plotted on a color scale defined by the P and AP states. The droplet state is seen as an intermediate resistance state. The dashed red line marks the linear droplet nucleation boundary. In the bottom of (c), nucleation boundary slope vs NC area together with a linear fit (dashed line).

direction. The step value is about 60% of the total difference between the parallel (P) and the antiparallel (AP) states, consistent with a droplet, and its location moves linearly to higher current magnitudes if the field is increased, consistent with the stiffening of the SWs and the field dependence of the Slonczewski threshold current

for a spin transfer torque driven SW instability [25]. The inset shows the same resistance step after subtraction of the parabolic background. An additional direct indication of a droplet is the appearance of broadband low-frequency microwave noise, only observed in the intermediate resistance state, which arises due to the particle-like Brownian motion of the droplet underneath the nanocontact [3,5,11].

Figure 2(b) shows the droplet nucleation as the field is increased from 0.16 to 0.42 T at three different strong negative currents and compared to a field sweep at much lower current. Again, the droplet is characterized by an intermediate resistance value, which first decreases slowly with the field until it drops more rapidly towards the resistance value of the P state. The gradual collapse indicates mode hopping between the droplet and the P state. Just as in Fig. 2(a), the droplet is again accompanied by the appearance of broadband low-frequency microwave noise.

In our all-perpendicular geometry—where the two magnetizations and the applied magnetic field are aligned with the film normal—the high-frequency precession of the droplet does not generate any microwave signal since the projection of the precessing spins onto the fixed layer magnetization remains constant in time. We can, however, detect the precession by tilting the applied field towards the film plane, creating a substantial noncollinearity between the free and the fixed layers magnetizations and hence a time-dependent variation of the STNO resistance. The inset in Fig. 2(b) shows a microwave measurement in a field

applied at 30° where a strong high-frequency droplet signal is indeed observed. It is noteworthy that the accompanying low-frequency noise is both much broader (0–2 GHz) and stronger compared to perpendicular fields, indicative of a strong drift instability in tilted fields and a highly stable droplet in the perpendicular case.

We have reproduced this general droplet behavior in a large number of STNOs having different nanocontact diameters. Figure 2(c) shows the corresponding current density or field state diagrams of the free layer magnetization in six different STNOs with diameters ranging from 50 to 150 nm, as measured by the normalized STNO resistance (the STNO resistance varies from 6.6Ω for a 50 nm NC diameter (d_{NC}) to 2.7Ω for $d_{\text{NC}} = 150$ nm). In all STNOs, the AP state either switches into the P state at low current magnitudes or into a droplet at high current magnitudes. The droplet nucleation boundary shows a linear dependence on both current and field. The figure in the bottom of Fig. 2(c) shows the slope of the nucleation boundary plotted vs the nanocontact area, confirming that the current density governs the droplet nucleation.

We now turn to our central result—the scanning transmission X-ray microscopy (STXM) measurements (see Supplemental Material [32] for details) on an 80 nm membrane STNO [Fig. 3(a)]. Overall, membrane and nonmembrane STNOs showed very similar electrical behavior. Figure 3(b) shows the resulting spatial STXM map of the m_z component of the Ni moments normalized to

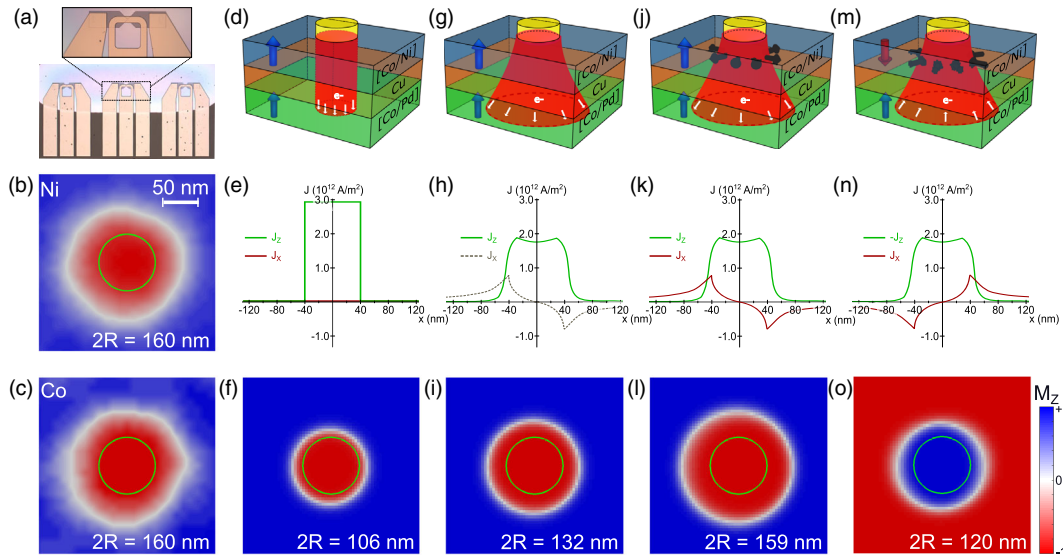


FIG. 3. (a) Photograph of three STNOs on a SiN membrane. (b), (c) Spatial STXM maps of the m_z component of the Ni (b) and Co (c) moments of the free layer, where the green circle outlines the nanocontact. Both STXM maps are obtained at -15 mA and in 0.18 T. Both maps reveal a fully reversed droplet with a diameter of about 160 nm. (d) Cartoon of the STNO with the current (red) flowing only in the perpendicular direction underneath the nanocontact (yellow). (e) Plots of the perpendicular (green) and lateral (red) current vs x coordinate. (f) Micromagnetic simulation of the resulting droplet. (g)–(i) Same as in (d)–(f) but with a realistic lateral current spread. The micromagnetic simulation includes the realistic spatial profile of the perpendicular current density but ignores the Zhang-Li torque from the lateral current. (j)–(l) Same as in (g)–(i) with the Zhang-Li torque included. (m)–(o) Same for a droplet in the AP state, including both the current spread and the Zhang-Li torque.

the up and down states well outside of the droplet region. The map reveals an essentially fully reversed droplet core with a well defined circular shape. The droplet diameter is approximately 160 nm, i.e., almost twice as large as the nominal NC diameter. Figure 3(c) shows the same analysis using the Co moment. As we have a signal from Co moments both in the free and the fixed layers and the normalization procedure switches both the free and the fixed layers, a second normalization step was done using the relative Co content in the free and the fixed layers, respectively. The spatial map of the m_z component of the free layer Co moments corroborates the conclusions drawn from the Ni signal—a fully reversed core and a diameter of 160 nm. In addition, we find that the minor deviations of the droplet perimeter from a perfect circle are uncorrelated between the Ni and Co maps. These deviations can therefore be ascribed to measurement noise and are not intrinsic to the droplet. The droplet is hence even more circular than what the individual maps would indicate on their own.

It is noteworthy that our direct measurement of the droplet diameter yields a much larger droplet than predicted by theory and micromagnetic simulations [3]. As a direct comparison, Fig. 3(f) shows a micromagnetic simulation of a droplet using the material parameters of our device. However, both theory and simulations assume a perfect cylindrical current distribution underneath the nanocontact [Figs. 3(d) and 3(e)], whereas recent experimental and numerical results indicate a large lateral current spread resulting in spin transfer torque over an area greater than the nanocontact [40]. While including this lateral current spread [Figs. 3(g) and 3(h)] indeed yields a 26 nm larger droplet diameter [Fig. 3(i)], the simulated droplet is still significantly smaller than in the experiment. The larger area of Slonczewski antidamping torque is hence not sufficient to explain our STXM observations.

The remaining large discrepancy can instead be resolved by also taking into account the Zhang-Li torque [41,42] from the in-plane current exerting an outward pressure on the droplet perimeter [Fig. 3(j)]. While this is the torque responsible for in-plane current induced domain wall (DW) motion, it has until now been ignored in STNOs. Steady-state DW motion is dominated by the nonadiabatic torque at currents below the Walker breakdown [42,43] and by the adiabatic term at currents well above the Walker breakdown [43]. In the former case, the spins inside the moving DW remain static (in the reference frame of the moving DW), while in the latter they precess. The precessing droplet perimeter, although pinned to the vicinity of the nanocontact, is hence a two-dimensional version of a moving DW well above the Walker breakdown, and the outward pressure should be dominated by the adiabatic torque. Including both the Slonczewski and the adiabatic Zhang-Li torque in our micromagnetic simulations, we can indeed recover the experimentally observed droplet size using realistic material parameters [Fig. 3(l)]. It is noteworthy that

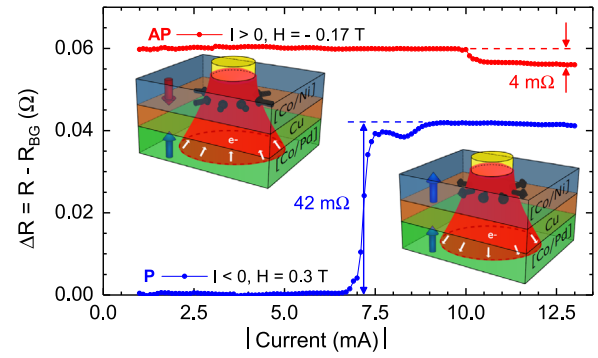


FIG. 4. The red data show how a droplet is nucleated from an AP state at +10 mA. The blue data show an ordinary droplet nucleated from the P state by a negative current. The resistance step with each droplet is highlighted by the red (AP) and blue (P) arrows, respectively. The insets show the corresponding magnetic state and the directions of the current and the pressure from the Zhang-Li torque.

the addition of a realistic nonadiabatic torque term had only a limited impact on the droplet size (≈ 2 nm), again confirming that the adiabatic torque dominates.

We can further test the validity of including the Zhang-Li torque by nucleating a droplet from the AP state since the current polarity must then be reversed to achieve antidamping Slonczewski torque. The opposite sign of the current also reverses the sign of the Zhang-Li torque; i.e., instead of an outward pressure, the droplet perimeter will now experience an inward pressure and the droplet should shrink. This is indeed observed in our micromagnetic simulations [Fig. 3(o)] where the droplet diameter is now 12 nm smaller than without the Zhang-Li torque and much smaller than the droplet in the P state (see Supplemental Material [32] for details of simulation parameters and equations).

As a final experimental confirmation, we can also directly nucleate and electrically measure a droplet in the AP state. As can be seen in Fig. 4, the resistance drop associated with the droplet nucleation in the AP state is an order of magnitude smaller in magnitude than the corresponding resistance increase of the droplet in the P state. This clearly indicates a much smaller droplet in the AP state compared to the P state, which corroborates our droplet model.

In conclusion, we have demonstrated stable and fully reversible magnetic droplet solitons in all-perpendicular spin torque nano-oscillators. Using scanning transmission X-ray microscopy, we find that the droplet diameter is almost twice that of the nanocontact and hence much larger than expected from droplet theory. By extending the original droplet theory to also account for lateral current spread, we attribute the large droplet size to in-plane Zhang-Li torque acting on the droplet perimeter. Micromagnetic simulations incorporating both the current spread and the adiabatic Zhang-Li torque closely reproduce

the droplet size. In the light of these new results, we expect that a correct treatment of both current spread and Zhang-Li torque will have important consequences not only for droplets but for any highly nonuniform static or dynamic state underneath a nanocontact.

This work was partially supported by the ERC Starting Grant No. 307144 “Mustang”, the Swedish Foundation for Strategic Research (SSF) Successful Research Leaders program, the Swedish Research Council (VR), the Göran Gustafsson Foundation, and the Knut and Alice Wallenberg Foundation. Helmholtz Zentrum Berlin is acknowledged for allocating beam time at the BESSY II synchrotron radiation facility. Financial support by Baden-Württemberg Stiftung in the framework of Kompetenznetz Funktionelle Nanostrukturen is gratefully acknowledged.

S. C. and Q. T. L. contributed equally to this work.

*Corresponding author.

johan.akerman@physics.gu.se

- [1] H.-B. Braun, *Adv. Phys.* **61**, 1 (2012).
- [2] B. Ivanov and A. Kosevich, *Sov. Phys. JETP* **45**, 1050 (1977).
- [3] M. A. Hoefler, T. J. Silva, and M. W. Keller, *Phys. Rev. B* **82**, 054432 (2010).
- [4] E. Iacocca, R. K. Dumas, L. Bookman, M. Mohseni, S. Chung, M. A. Hoefler, and J. Åkerman, *Phys. Rev. Lett.* **112**, 047201 (2014).
- [5] S. M. Mohseni, S. R. Sani, J. Persson, T. N. A. Nguyen, S. Chung, Y. Pogoryelov, P. K. Muduli, E. Iacocca, A. Eklund, R. K. Dumas, S. Bonetti, A. Deac, M. A. Hoefler, and J. Åkerman, *Science* **339**, 1295 (2013).
- [6] F. Macià, D. Backes, and A. D. Kent, *Nat. Nanotechnol.* **9**, 992 (2014).
- [7] S. Mohseni, S. Sani, R. Dumas, J. Persson, T. A. Nguyen, S. Chung, Y. Pogoryelov, P. Muduli, E. Iacocca, A. Eklund, and J. Åkerman, *Physica B (Amsterdam)* **435**, 84 (2014).
- [8] S. Chung, S. M. Mohseni, S. R. Sani, E. Iacocca, R. K. Dumas, T. N. Anh Nguyen, Y. Pogoryelov, P. K. Muduli, A. Eklund, M. Hoefler, and J. Åkerman, *J. Appl. Phys.* **115**, 172612 (2014).
- [9] S. Lendínez, N. Statuto, D. Backes, A. D. Kent, and F. Macià, *Phys. Rev. B* **92**, 174426 (2015).
- [10] S. Chung, S. M. Mohseni, A. Eklund, P. Dürrenfeld, M. Ranjbar, S. R. Sani, T. N. Anh Nguyen, R. K. Dumas, and J. Åkerman, *Low Temp. Phys.* **41**, 833 (2015).
- [11] S. Chung, A. Eklund, E. Iacocca, S. M. Mohseni, S. R. Sani, L. Bookman, M. A. Hoefler, R. K. Dumas, and J. Åkerman, *Nat. Commun.* **7**, 11209 (2016).
- [12] D. Xiao, V. Tiberkevich, Y. H. Liu, Y. W. Liu, S. M. Mohseni, S. Chung, M. Ahlberg, A. N. Slavin, J. Åkerman, and Y. Zhou, *Phys. Rev. B* **95**, 024106 (2017).
- [13] S. Lendínez, J. Hang, S. Vélez, J. M. Hernández, D. Backes, A. D. Kent, and F. Macià, *Phys. Rev. Applied* **7**, 054027 (2017).
- [14] A. Slavin and V. Tiberkevich, *Phys. Rev. Lett.* **95**, 237201 (2005).
- [15] S. Bonetti, V. Tiberkevich, G. Consolo, G. Finocchio, P. Muduli, F. Mancoff, A. Slavin, and J. Åkerman, *Phys. Rev. Lett.* **105**, 217204 (2010).
- [16] V. E. Demidov, S. Urazhdin, and S. O. Demokritov, *Nat. Mater.* **9**, 984 (2010).
- [17] S. Bonetti, V. Puliafito, G. Consolo, V. S. Tiberkevich, A. N. Slavin, and J. Åkerman, *Phys. Rev. B* **85**, 174427 (2012).
- [18] V. Demidov, S. Urazhdin, H. Ulrichs, V. Tiberkevich, A. Slavin, D. Baither, G. Schmitz, and S. Demokritov, *Nat. Mater.* **11**, 1028 (2012).
- [19] R. K. Dumas, E. Iacocca, S. Bonetti, S. R. Sani, S. M. Mohseni, A. Eklund, J. Persson, O. Heinonen, and J. Åkerman, *Phys. Rev. Lett.* **110**, 257202 (2013).
- [20] R. Dumas, S. Sani, S. Mohseni, E. Iacocca, Y. Pogoryelov, P. Muduli, S. Chung, P. Dürrenfeld, and J. Åkerman, *IEEE Trans. Magn.* **50**, 4100107 (2014).
- [21] T. Chen, R. K. Dumas, A. Eklund, P. K. Muduli, A. Houshang, A. A. Awad, P. Dürrenfeld, B. G. Malm, A. Rusu, and J. Åkerman, *Proc. IEEE* **104**, 1919 (2016).
- [22] M. Tsoi, A. G. M. Jansen, J. Bass, W.-C. Chiang, M. Seck, V. Tsoi, and P. Wyder, *Phys. Rev. Lett.* **80**, 4281 (1998).
- [23] M. Tsoi, A. G. M. Jansen, J. Bass, W.-C. Chiang, V. Tsoi, and P. Wyder, *Nature (London)* **406**, 46 (2000).
- [24] W. H. Rippard, M. R. Pufall, S. Kaka, S. E. Russek, and T. J. Silva, *Phys. Rev. Lett.* **92**, 027201 (2004).
- [25] J. C. Slonczewski, *J. Magn. Magn. Mater.* **195**, L261 (1999).
- [26] M. Madami, S. Bonetti, G. Consolo, S. Tacchi, G. Carlotti, G. Gubbiotti, F. B. Mancoff, M. A. Yar, and J. Åkerman, *Nat. Nanotechnol.* **6**, 635 (2011).
- [27] M. Madami, E. Iacocca, S. Sani, G. Gubbiotti, S. Tacchi, R. K. Dumas, J. Åkerman, and G. Carlotti, *Phys. Rev. B* **92**, 024403 (2015).
- [28] A. Houshang, E. Iacocca, P. Dürrenfeld, S. R. Sani, J. Åkerman, and R. K. Dumas, *Nat. Nanotechnol.* **11**, 280 (2016).
- [29] W. H. Rippard, A. M. Deac, M. R. Pufall, J. M. Shaw, M. W. Keller, S. E. Russek, G. E. W. Bauer, and C. Serpico, *Phys. Rev. B* **81**, 014426 (2010).
- [30] S. M. Mohseni, S. R. Sani, J. Persson, T. N. Anh Nguyen, S. Chung, Y. Pogoryelov, and J. Åkerman, *Phys. Status Solidi RRL* **5**, 432 (2011).
- [31] D. Backes, F. Macià, S. Bonetti, R. Kukreja, H. Ohldag, and A. D. Kent, *Phys. Rev. Lett.* **115**, 127205 (2015).
- [32] See Supplemental Material at <http://link.aps.org/supplemental/10.1103/PhysRevLett.120.217204> for more information, which includes Refs. [33–39].
- [33] D. Nolle, M. Weigand, P. Audehm, E. Goering, U. Wiesemann, C. Wolter, E. Nolle, and G. Schtz, *Rev. Sci. Instrum.* **83**, 046112 (2012).
- [34] W. Rasband, ImageJ (1997–2015).
- [35] A. Vansteenkiste, J. Leliaert, M. Dvornik, M. Helsen, F. Garcia-Sanchez, and B. Van Waeyenberge, *AIP Adv.* **4**, 107133 (2014).
- [36] J. Heinen, D. Hinzke, O. Boulle, G. Malinowski, H. J. M. Swagten, B. Koopmans, C. Ulysse, G. Faini, and M. Kläui, *Appl. Phys. Lett.* **99**, 242501 (2011).

- [37] C. Burrowes, A. P. Mihai, D. Ravelosona, J.-V. Kim, C. Chappert, L. Vila, A. Marty, Y. Samson, F. Garcia-Sanchez, L. D. Buda-Prejbeanu, I. Tudosa, E. E. Fullerton, and J.-P. Attané, *Nat. Phys.* **6**, 17 (2010).
- [38] M. D. Stiles and A. Zangwill, *Phys. Rev. B* **66**, 014407 (2002).
- [39] K. Xia, P. J. Kelly, G. E. W. Bauer, A. Brataas, and I. Turek, *Phys. Rev. B* **65**, 220401 (2002).
- [40] S. A. H. Banuazizi, S. R. Sani, A. Eklund, M. M. Naiini, S. M. Mohseni, S. Chung, P. Dürrenfeld, B. G. Malm, and J. Åkerman, *Nanoscale* **9**, 1896 (2017).
- [41] Z. Li and S. Zhang, *Phys. Rev. B* **70**, 024417 (2004).
- [42] S. Zhang and Z. Li, *Phys. Rev. Lett.* **93**, 127204 (2004).
- [43] A. Thiaville, Y. Nakatani, J. Miltat, and Y. Suzuki, *Europhys. Lett.* **69**, 990 (2005).